Editors' Suggestion

Conductance and adhesion in an atomically precise Au-Au point contact

Lukas Gerhard[1,*] and Wulf Wulfhekel[1,2]

[1]*Institute of Quantum Materials and Technology, Karlsruhe Institute of Technology (KIT), D-76344 Eggenstein-Leopoldshafen, Germany*

[2]*Physikalisches Institut, Karlsruhe Institute of Technology (KIT), D-76131 Karlsruhe, Germany*

(Received 4 November 2019; published 30 January 2020)

Comprehension of electrical and mechanical properties of atomic-sized metal contacts are of central importance for a number of different fields, e.g., the development of interconnects in nanoelectronics, the description of friction on the nanoscale, and break-junction experiments. Au-Au nanocontacts are experimentally particularly suited because of the chemical inertness and serve as a valuable testbed for charge transport in the quantum regime. Here we use the tip of a low-temperature scanning tunneling microscope to form atomic contacts with a reconstructed Au(111) surface. As both electrodes are perfectly stable throughout 19 000 individual measurements, the atomic configuration of the point contact can be precisely controlled by variation of the tip position with respect to the substrate atoms and the reconstruction domains with different stacking. This allows us to reveal the influence of the two last atomic layers of each electrode on the conductance and the stiffness of the junction. Four different conductance regimes can be distinguished and explained by two atomic conductance channels. The stiffness of the junction can be inferred from the adhesion hysteresis that is reduced at threefold hollow sites and closed-packed domains of the reconstructed surface. Our experimental results will allow profound tests of atomic-scale theoretical simulations in the field.

DOI: 10.1103/PhysRevB.101.035429

I. INTRODUCTION

The understanding of the complex interplay between distance, force, and electron transport during formation and breaking of a contact between two metallic electrodes is of fundamental interest for nanoscale electronics. When the smallest wires come to the atomic scale, the electrical conductance is governed by quantum effects. The conductance of such atomic contacts can be studied by stretching a thin gold wire. Then the conductance decreases in a stepwise manner and just before the contact breaks, it typically takes a conductance value of $G_0 \approx 2e^2/h$ (e: electron charge, h: Planck's constant), which is interpreted as a single atomic contact [1–12]. This well known effect is widely used to calibrate the distance between the two electrodes in break-junction experiments. When the two electrodes are brought together, the contact closes again. Often the atomic contact forms and breaks at slightly different nominal distance during the approach and retraction of the two electrodes. It is believed that an abrupt jump into contact (JIC) is caused by atomic rearrangements in the electrodes [2,11–13]. However, this rearrangement is not necessarily a plastic deformation and reproducible contact curves have been found in mechanically annealed break junctions [14,15]. Then the hysteresis between JIC and jump out of contact (JOC) results from the competition of the elasticity and the adhesion between the last atoms of both electrodes. In this case, the hysteresis could be related to the stiffness of the electrodes within a simple model [14]. While break-junction experiments lack the possibility of controlled lateral displacement, the formation of single atom contacts has also been widely studied in scanning tunneling microscopy (STM) which allows us to study one of the two electrodes prior to contact formation [16] and to map the surface in the contact regime [17]. Reproducible contact formation to the Au(111) lattice with a gold tip or through a single gold adatom, however, could not be achieved without plastic deformation of the tip or deposition of atoms onto the surface and therefore the atomic location of the contact formation remained unknown [11,12,17]. Furthermore, experiments on the contact formation of an atomically sharp tip with a reconstructed Au(111) surface showed no difference between fcc and hcp domains [11]. Recently, the site-dependent conductance of a Pb-Pb junction has been studied in the STM configuration [16]. Discrepancies in conductance curves were found for on-top and hollow site positions and a difference between fcc and hcp hollow sites was identified. However, JIC/JOC or a hysteresis between approach and retraction curves was not observed in this system.

Here we present low-temperature STM measurements of reproducible contact formation in the prototypical Au junctions, i.e., between a Au coated tip and a reconstructed Au(111) surface. Because plastic deformation of neither the tip nor the sample surface occurred in our measurement, we are able to map all features of the adhesion hysteresis curve, including JIC/JOC, with atomic resolution all across the fcc and hcp domains of the herringbone reconstruction. Our results reveal the influence of the two last atomic layers of each electrode on the electrical conductance and the mechanical stiffness of the junction.

II. METHODS

A. STM experiments

STM measurements were carried out in a home-built STM in UHV at a temperature of 5.2 K. The STM tip was prepared

*lukas.gerhard@kit.edu

by chemical etching of a tungsten wire and by repeated dipping into the gold surface. The Au(111) single-crystal surface was cleaned by several cycles of Ar^+ sputtering and annealing to 700 K. The voltage is applied to the sample. The experiment comprises a measurement of the conductance on a three-dimensional mesh of $720 \times 27 \times 100$ points on a volume of $9 \times 0.24 \times 0.23\ \mathrm{nm}^3$ in x, y (lateral) and z direction (distance), respectively. The feedback loop was not used in the present work, i.e., all conductance versus distance [$G(z)$] curves start at the same plane parallel to the surface. In this work, the tip position z is defined as the offset of the overall tip from its initial z position. It does not include eventual elastic deformation of tip or sample and thus it does not reflect the distance between the last atom of the tip and the last atom of the sample. The conductance was measured at a low bias of 4 ± 0.4 mV in order to minimize Joule heating or structural modifications by the electric field [18,19].

The reconstruction of the Au(111) surface leads to a characteristic "herringbonelike" pattern of bright ridges (transition area), separating areas of face centered cubic (fcc) and hexagonal closed-packed (hcp) stacking [20,21]. The measurement area was chosen so that fcc, transition, and hcp domains were covered, which allows a straightforward and unambiguous comparison of conductance and hysteretic characteristics for different atomic configurations of the junction.

B. Stiffness simulation

The positions of the atoms in the herringbone reconstruction were taken from [21]. The simulation was being carried out using the atomic simulation environment (ASE) [22]. Each atom was moved vertically by 180 pm and the nine nearest neighbors were relaxed using the FIRE algorithm [23]. Relaxing the whole unit cell would imply simulation of the herringbone reconstruction, which is beyond the scope of this simulation. The stiffness was obtained by fitting the resulting parabola.

III. RESULTS AND DISCUSSION

To begin, we describe a single $G(z)$ curve: the current was recorded while the STM tip was approached towards the surface [black curve in Fig. 1(a)] and was retracted back to its initial position [red curve in Fig. 1(a)]. The apex of the tip and the surface jump into contact at a certain distance [black dashed line at $z_{\mathrm{JIC}} \approx -220$ pm in Fig. 1(a)], and the conductance abruptly increases to a value slightly above $G_0 = 2e^2/h$. Approaching the tip further towards the sample, we find a second jump [black dashed line at $z_{\mathrm{JIC2}} \approx -250$ pm in Fig. 1(a)] where the conductance increases to $G = 2\,G_0$. Upon retraction, at larger distances between tip and sample, the conductance is first reduced back to about $1\,G_0$ [red dashed line at $z_{\mathrm{JOC2}} = -220$ pm in Fig. 1(a)] and upon further retraction it finally drops to the tunneling conductance [red dashed line at $z_{\mathrm{JOC}} = -170$ pm in Fig. 1(a)]. We thus observed two conduction plateaus, both in the approach and retraction curves [24].

Such $G(z)$ curves were recorded on an image of 720×27 pixels, which allows us to derive fully consistent maps at constant height and constant conductance. The absence of any plastic deformation of the electrodes allows us to identify the influence of the local crystallographic structure of the sample. Maps of constant conductance provide a possibility to compare our data to normal constant current STM images. Therefore, the position z, at which a certain conductance is reached, is plotted for each pixel. Note that these maps are different to normal constant height images or measurements in contact presented in [17] in view of the fact that here the STM tip is retracted after each pixel. Figure 1(b) shows such a map in the tunneling regime at a conductance of $0.045\,G_0$ derived from the approach (app) curves. The typical corrugation of the herringbone reconstruction allows us to assign fcc, hcp, and transition areas. Note that the image was recorded at an angle of about 83° with respect to the ridges of the reconstruction. Next, we discuss a conductance of $0.35\,G_0$ which is slightly higher than the maximum conductance in the tunneling regime. That is, the corresponding map shown in Fig. 1(c) indicates the z position at which JIC occurs. In the tunneling regime, it is questionable to correlate the observed corrugation [see Fig. 1(b)] with the real corrugation of the surface atoms [25]. The map of z_{JIC} plotted in Fig. 1(c), however, is a reasonable definition of the sample surface on the atomic scale as it is important for the modeling of friction on the nanoscale [26]. This map allows us to assign the positions of the surface atoms, which is relevant for the further interpretation of our data.

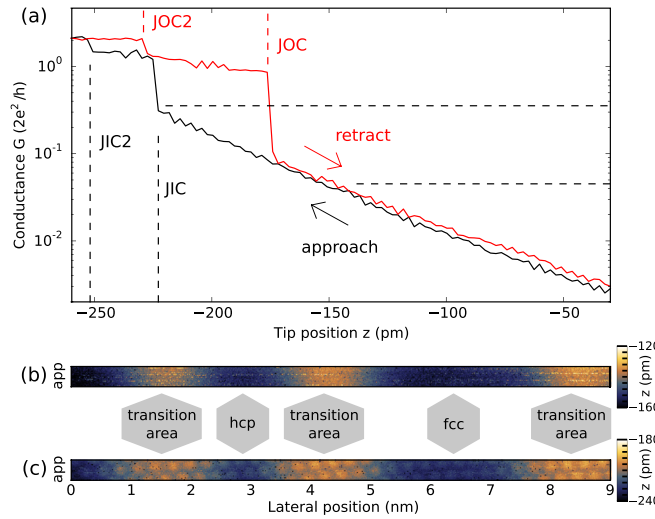

FIG. 1. (a) Typical $G(z)$ curve for approach (black) and retraction (red) of the STM tip. Jumps into contact (JIC, JIC2) that lead to higher conductance during approach are indicated by black dashed lines. Jumps out of contact (JOC, JOC2) that lead to lower conductance during retraction are indicated by red dashed lines. (b) and (c) Reconstructed constant current images: Slices of the data set at a conductance of (b) $0.045\,G_0$ and (c) $0.35\,G_0$ [indicated by horizontal dashed lines in (a)] taken from the approach curves (app).

A. Contact regimes

In the following section it will be shown that the site-dependent conductance behavior of the junction can be explained by a simple atomistic model including the conductance contributions of the last and the second last tip atoms

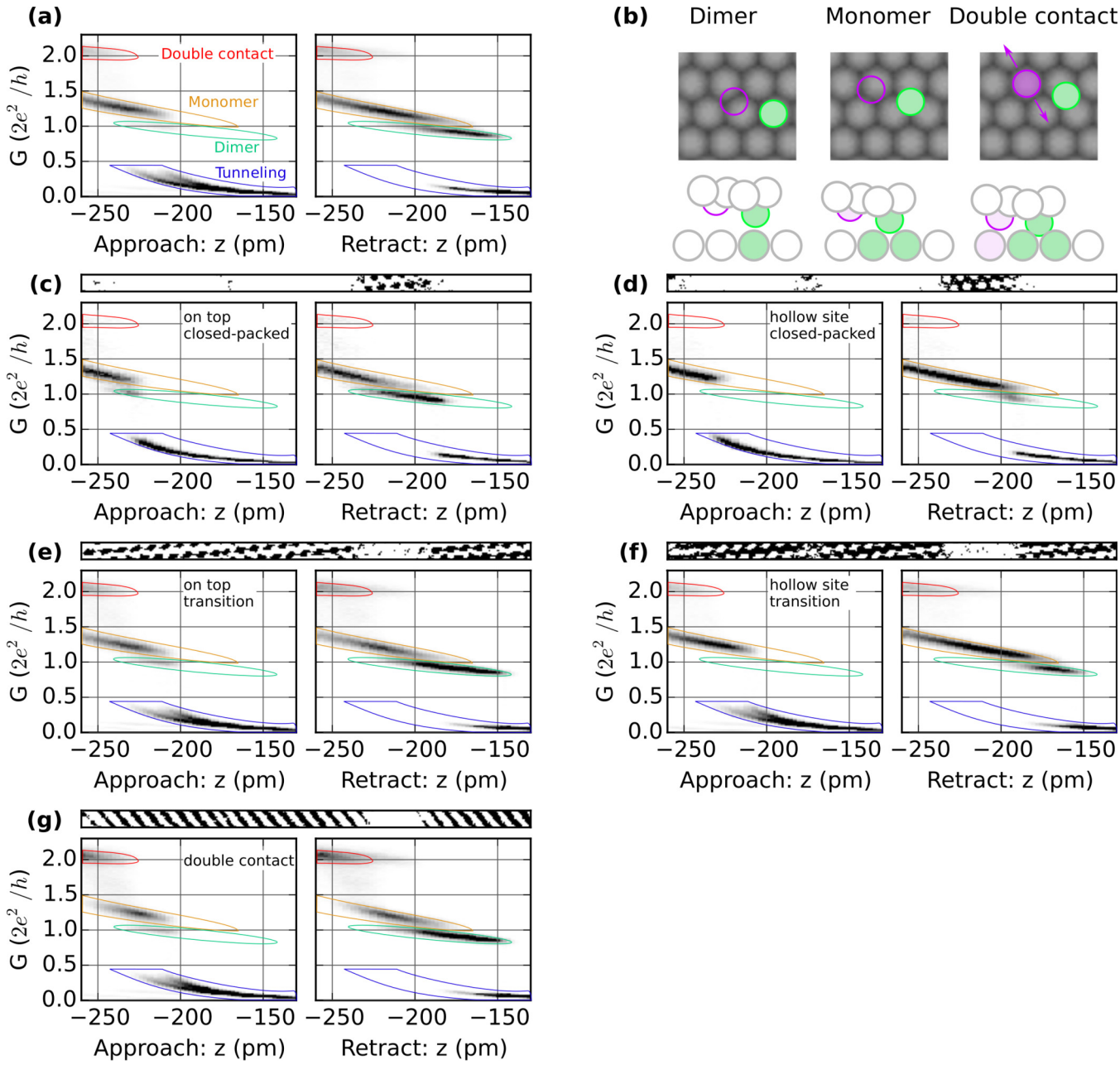

FIG. 2. 2D histogram of the conductance versus tip position during contact formation. (a) Including all $G(z)$ curves. The four different contact regimes are encircled as a guide to the eye. (b) Ball model for the different contact regimes: The last tip atom is shown in green, the second last tip atom in pink. Arrows indicate the direction of higher flexibility of the tip. (c) On-top site, closed-packed, (d) hollow site, closed-packed, (e) on-top site, transition area, (f) hollow site, transition area, and (g) positions that show double contact.

(G_{t1}, G_{t2}) and the site-dependent elasticity of the surface. All approach and retraction curves were plotted in a 2D histogram without any treatment of the data [see Fig. 2(a)]. At first sight, it can be seen that all curves show clear JIC and JOC at a conductance of about 1 G_0. A closer look reveals four different distinct contact regimes with characteristic $G(z)$ dependence. As a guide to the eye, the different contact regimes are encircled with colored lines [see Fig. 2(a)].

Owing to the lateral resolution of our measurement, we are able to prove that the observed conductance regimes correspond to the atomic configurations predicted theoretically by Untiedt *et al.* [27,28]: Therefore, we study the contact formation for different starting configurations of the atomic structure of the junction by approaching the surface at different lateral positions. We distinguish six different subsets of the data as indicated by the black masks: On-top [Figs. 2(c) and 2(e)] or hollow sites [Figs. 2(d) and 2(f)], at the closed-packed [Figs. 2(c) and 2(d)], or the transition area of the reconstruction [Figs. 2(e) and 2(f)]. Additionally, the positions where a jump to $G = 2\,G_0$ is observed are mapped [Fig. 2(g)]. Following the nomenclature by Untiedt *et al.* [27,28], we identify the following atomic configurations of the electrodes and the corresponding conductance regimes: The lowest conductance $G_{\text{total}} = G_{t1} + G_{t2}$ is observed in the tunneling regime where

$G_{t1} < 0.35\,G_0$, $G_{t2} \approx 0$ (encircled by purple lines in Fig. 2). When the tip approaches an on-top site [see Figs. 2(c) and 2(e)], JIC results in a diatomic gold wire (encircled by green lines in Fig. 2). This configuration is outlined in Fig. 2(b) and is expected to result in a conductance of $G_{t1} \approx 1\,G_0$, $G_{t2} \approx 0$ (simulation by Untiedt *et al.*: $0.87\,G_0$). When stretching the junction, JOC happens almost exclusively via the dimer configuration irrespective of the atomic configuration before JIC, which is due to the fact that short range forces prior to JOC are drastically higher than the ones prior to JIC. Higher conductance values are related to the formation of a monomer (encircled by orange lines in Fig. 2), that is a single restriction of one atom in diameter. The increased conductance of the monomer compared to the dimer is explained by taking into account the additional tunneling conductance of atoms beyond the actual contact atom ($G_{t1} \approx 1\,G_0$, $G_{t2} \approx G_{\text{tunneling}}$, simulation by Untiedt *et al.*: $1.6\,G_0$). On the on-top sites, approaching the tip in the contact regime leads to an abrupt transition from the dimer to the monomer configuration. This transition begins when the short range forces between the last tip atom and a second sample atom overcame the (lateral) elastic forces. When the tip approaches a hollow site, JIC directly results in the monomer configuration (encircled by orange lines in Fig. 2) with a conductance above $1\,G_0$ [see Figs. 2(d) and 2(f)]. In this picture, the slope of dimer and monomer regimes is explained by the distance dependent variation of the tunneling contribution of the second tip atom. The highest conductance regime is explained by a double contact where both $G_{t1} \approx 1\,G_0$ and $G_{t2} \approx 1\,G_0$ (simulation: $2.04\,G_0$). In our experiment, this conductance plateau at $G_{\text{Double contact}} = 2\,G_0$ (encircled by red lines in Fig. 2) is found in about half of the transition area [see Fig. 2(g)] and is separated from the monomer regime by a clear jump in conductance. The mask in Fig. 2(g) shows the positions where the double contact is observed. The corresponding pattern cannot be explained by the symmetry of the surface, so it must relate to the shape of the tip electrode as proposed in Fig. 2(b): Only for particular positions of the tip with respect to the atomic lattice, the asymmetric elasticity of the tip electrode allows the second last tip atom to jump to the direct contact. Note that this simplified model which qualitatively explained the observations only holds true in the case of gold contacts where the electron transport is mediated by a single spherically symmetric s orbital [24].

B. Conductance of the junction at different sample positions

In the work by Kim and Hasegawa [16], the site specific conductance is compared at a plane parallel to the surface. In the case of a junction that shows JIC and JOC, to evaluate the site-dependent conductance, we map the conductance $G_{\text{JIC+}}$ ($G_{\text{JOC−}}$) right after JIC (before JOC) in the approach (retraction) curve [see Figs. 3(a) and 3(b)] [29]. $G_{\text{JIC+}}$ shows higher values than $G_{\text{JOC−}}$ at all positions due to the supplemental tunneling conductance G_{t2} of the second last tip atom after JIC. Figure 3(a) displays the conductance mapping at the position right after JIC and reveals an atomically resolved lattice with minimum conductance at the on-top sites.

With the representation of the data in the 2D histograms (Fig. 2) in mind, this can be understood as a lower

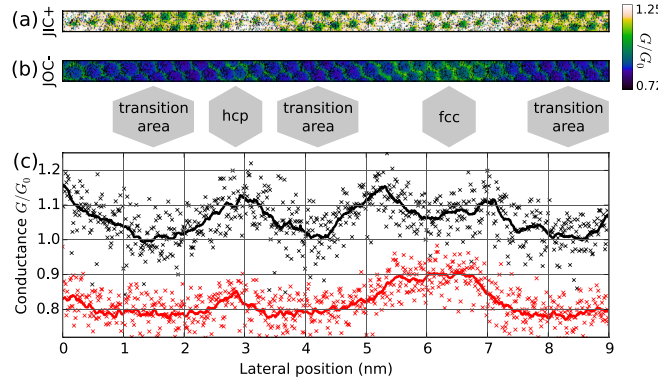

FIG. 3. (a) Map of the conductance just after JIC ($G_{\text{JIC+}}$) and (b) just before JOC ($G_{\text{JOC−}}$). (c) Column averaged values of $G_{\text{JIC+}}$ (black crosses and black line) and $G_{\text{JOC−}}$ (red crosses and red line).

conductance of the dimer configuration (green circles in Fig. 2) as compared to the conductance of the monomer configuration (orange circles in Fig. 2). In other words, G_{t2} of both JOC and JIC shows higher values at hollow sites, simply because the contact forms and breaks at closer distances between tip and sample so that the second last tip atom is closer to the sample. We do not observe a significant difference between hcp and fcc hollow sites that we could assign to the atomic configuration of the sample. As the tunneling contribution G_{t2} depends on the position of the second last tip atom (see also Fig. 4), statistical analysis of numerous measurements with different tips apices would be necessary in order to identify a possible difference between hcp and fcc hollow sites.

In order to visualize the variation across the reconstruction, the conductance maps Figs. 3(a) and 3(b) are averaged along the columns [black and red crosses in Fig. 3(c)] and smoothed using Savitzky-Golay filter along the lateral position [black and red curves in Fig. 3(c)]. At the transition regions (at $x \approx 1.5, 4, 8$ nm), both the column-averaged $G_{\text{JIC+}}$ (black crosses and black line) and $G_{\text{JOC−}}$ (red crosses and red line) are found to be lower than the conductance at hcp and fcc areas. This can be explained by the increased elastic deformation of the

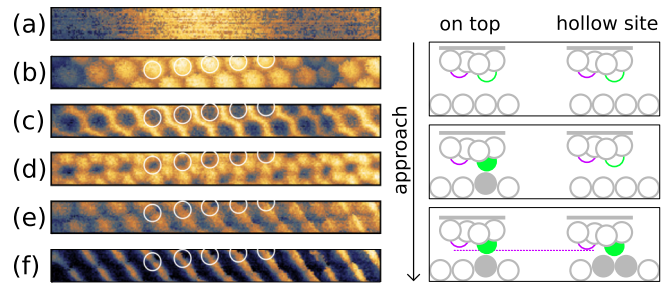

FIG. 4. Reconstructed constant current images: Slices of the data set at a conductance of (a) $0.04\,G_0$, (b) $0.35\,G_0$, (c) $0.94\,G_0$, (d) $1.15\,G_0$, (e) $1.24\,G_0$, and (f) $1.35\,G_0$. White circles indicate on-top positions for the last tip atom. The width of the images is 3.5 nm. The schematic on the right depicts the basic mechanism that leads to contrast reversal when approaching the tip. The nominal tip position is indicated by a thick gray line, the last (second last) tip atom is displayed in green (pink). For details see text.

surface at the transition areas which leads to JIC and JOC at larger distances between tip and sample than at the closed-packed areas. Therefore, G_{t2}, and consequently G_{total}, is lower at the transition areas. The reason for the local minimum of the conductance $G_{\text{JIC+}}$ in the middle of the fcc closed-packed area (at $x \approx 6$ nm), however, is unclear.

C. Contrast reversal in constant current topography

In previous STM topographic measurements performed in or close to the contact regime, it has been observed that the conductance is not always highest at the on-top positions of the substrate atoms [16,17,30]. The contrast reversal phenomenon has been speculated to be related to the larger adsorption energy of the manipulated atom at the hollow sites. Thus the probability to bridge the tunneling gap would became larger [30]. While Kim *et al.* related the contrast to a stronger attractive force between tip and sample at hollow sites [16], the mechanism leading to an increased conductance was unclear.

Our data show multiple changes of the contrast pattern in constant-current maps [derived from our $G(z)$ curves by plotting the position z, at which a certain conductance is reached], depending on the distance between tip and sample. Here we show that this contrast reversal is a natural consequence of the atomic model of the contact formation presented above.

Figures 4(a)–4(f) shows constant-current maps (corresponding to the apparent height) of the transition area derived from the retraction curves at conductance values of $0.04\,G_0$, $0.35\,G_0$, $0.94\,G_0$, $1.15\,G_0$, $1.24\,G_0$, $1.35\,G_0$. The schematic on the right of Fig. 4 shows the situation of the last few tip atoms and the surface atoms when approaching the tip. Please note that for clarity, this schematic depicts the situation of same nominal tip position (indicated by a thick gray line) for on top and hollow site positions. In the tunneling regime at $G = 0.04\,G_0$ [Fig. 4(a)] almost no atomic contrast is visible. $G = 0.35\,G_0$ [Fig. 4(b)] is reached as soon as a direct contact is formed. At the on-top positions (indicated by white circles) the dimer configuration of the contact is stable at the largest distance between tip and sample (largest z) and therefore the on-top positions show larger apparent height [bright spots in Fig. 4(b)]. A conductance $G = 0.94\,G_0$ or higher [Figs. 4(c)–4(e)] additionally requires a significant tunneling contribution G_{t2} from the second last tip atom. G_{t2} depends on the distance between the second last tip atom and the surface. This distance, in turn, is determined by the overall tip position z (which is plotted as the "apparent height" in the constant current topography) and the elastic elongation of the tip. In contact, this elastic elongation of the tip mainly depends on the vertical position of the last tip atom. At the bridge positions, the last tip atom lies lower than at the on-top positions and therefore, the elastic elongation of the tip and the tunneling contribution G_{t2} from the second last tip atom are more significant (see also the schematic on the right of Fig. 4). Consequently, the conductance of $G = 0.94\,G_0$ is obtained at larger tip position z (larger apparent height) at the bridge position than at the on-top positions, which explains the contrast reversal from Fig. 4(b) to 4(c). In the same way, the geometrically even deeper threefold hollow sites show the largest apparent height at a conductance of $G = 1.15\,G_0$ [see Fig. 4(d)]. A possible increased binding energy at hollow sites due to higher coordination of the tip atom with the surface atoms would enhance this effect. When the tip is even closer, not only the distance between second last tip atom and the sample, but also the lateral position of the second last tip atom with respect to the surface atoms determines the conductance. At a conductance of $G = 1.24\,G_0$ [see Fig. 4(e)], the second last tip atom eventually leads to an atomically resolved lattice which is shifted with respect to Fig. 4(b) by the lateral distance between the last and the second last tip atom [see Fig. 4(e)]. At even smaller z, also the second last tip atom jumps into contact when it is above on-top positions or "backslash" bridge positions which can be seen as bright ridges in Fig. 4(f). Note that these topographies are derived from a consistent set of I-z curves, which fully excludes any tip change as the origin of the different patterns.

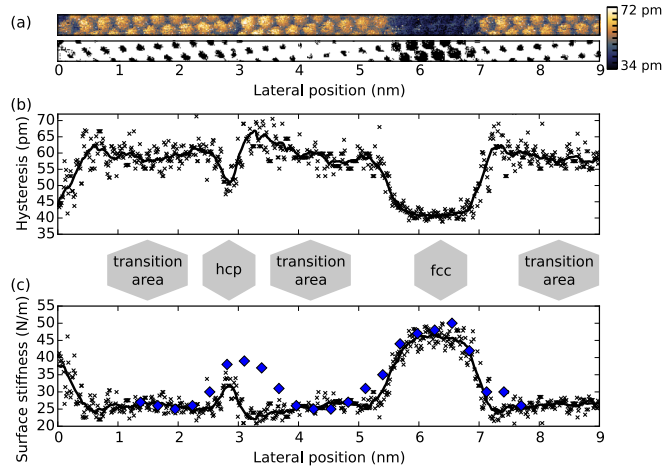

FIG. 5. (a) Hysteresis between JIC and JOC (upper panel), mask for on-top positions (lower panel). (b) Column averaged variation along the x direction (bottom panel). The solid line is smoothed using Savitzky-Golay filter. (c) Surface stiffness derived from the hysteresis plotted in (b) for $k_{\text{tip}} = 12$ N/m. The solid line is smoothed using Savitzky-Golay filter. Blue diamonds are the corresponding values obtained from the simulation (for details see Methods section).

D. Hysteresis and surface stiffness

Besides the conductances before and after the jumps, the approach-retract curves are characterized by the nominal vertical position of the tip at which these jumps occur. Here we discuss the width of the hysteresis, that is $\Delta z = z(\text{JOC}) - z(\text{JIC})$. This hysteresis is related to the combination of the finite stiffness of the two electrodes and the short range forces that quickly increase upon contact formation. The width of the hysteresis depends on the material, the current density [5], and the geometry of the two electrodes [27]. In previous STM studies, the plastic deformation of the tip electrode upon contact formation lead to variations of z(JIC) of the order of 40 pm, which obscured any possible influence of the surface stacking on the hysteresis [11]. Our data allows us to directly relate differences in the hysteresis to different stacking orders of the reconstructed Au(111) surface, as we can exclude any plastic deformation of the tip electrode. Figure 5(a) shows the corresponding map of Δz, that is the width of the hysteresis.

The variation of the hysteresis is correlated with the atomic lattice with maximums at on-top sites and minimums at hollow sites. While the monomer configuration found at JIC at the hollow-site positions [see Figs. 2(d) and 2(f)] probably results in a higher bond energy favoring a larger hysteresis, the increased geometrical stiffness of the junction dominates and leads to a smaller hysteresis. Interestingly, there is a clear difference between the closed-packed areas ($\Delta z \approx 40$ pm) and the transition areas ($\Delta z \approx 60$ pm). Intuitively, this can be explained by a higher stiffness of the closed-packed structure compared to the more open transition region where the surface atoms have a lower coordination. As has been shown by Trouwburst *et al.*, in a break-junction experiment [14], the hysteresis for situations with reproducible contact formation in the dimer configuration, i.e., for cases with no plastic deformation, allows us to derive the stiffness of the corresponding electrodes. It has been shown that the interaction between the last atoms of the two electrodes can be described using a so-called universal binding curve. As the equilibrium distance, the break force and the binding energy of a single gold-gold bond are known (see [6,14] and references therein), the stiffness of the electrodes is the only free parameter. Following this model we estimated the stiffness of the junction for each curve (each pixel in the maps). Since the model assumes a dimer configuration of the atomic contact, only on-top sites of the lattice were included in the analysis [see mask shown in lower panel in Fig. 5(a)]. In order to visualize the quantitative variation of the hysteresis across the reconstruction, the column-averaged variation (including only the on-top curves) along the long axis of our map is plotted in Fig. 5(b). The resulting stiffness of the whole junction, that is tip and surface in series, varies between 6.5 and 10 N/m. *A priori*, the stiffness of the tip electrode k_{tip} is unknown besides it is constant in our experiment. However, it seems reasonable to assume that the stiffness of the (sharp) tip is lower than that of the atomically flat single crystal surface k_{surface}, which narrows the range to $10 < k_{\mathrm{tip}} < 13$ N/m. Figure 5(c) (black crosses) shows the estimated surface stiffness k_{surface} derived from the column-averaged hysteresis [Fig. 5(b)] for $k_{\mathrm{tip}} = 12$ N/m. A simple simulation of the surface stiffness which measures the change in energy upon moving a single atom (see Methods), results in a surface stiffness k_{surface} in the range between 25 N/m at the transition region and 50 N/m at the fcc domain [blue diamonds in Fig. 5(c)]. This agrees with previous more sophisticated calculations for the closed-packed area (52 N/m found in [25]) and nicely reproduces the experimental values for a stiffness of the tip of $k_{\mathrm{tip}} = 12$ N/m. This value of k_{tip} fits well within the range of stiffnesses found in [14] and other break-junction experiments. With this, the reduced hysteresis on the closed-packed area translates into an increased stiffness of the surface.

IV. CONCLUSIONS

In conclusion, atomically resolved conductance-distance maps draw a consistent picture of the atomic details of contact formation of a Au tip to a reconstructed Au(111) surface. With the distance of JIC as the reference for contact, we mapped the topography of the Au(111) surface on the atomic scale that is relevant for the microscopic understanding of touching bodies. Furthermore, we were able to form contacts with different atomic configurations by approaching the surface at different lateral positions. This allowed us to confirm the sequence of four theoretically predicted conductance regimes which can be understood as a combination of the two conductance channels of the last and the second last tip atom. This simple model allowed us to explain the effect of multiple contrast reversals in STM images at high tunneling currents. We have experimentally derived the variation of the surface stiffness at the different stacking orders present at the reconstructed surface. Our results clearly show that on the atomic level, the spatially mapped values of apparent height and conductance cannot be assigned to the sample but result from the interplay of both electrodes. Finally, these results will allow us to test atomic-scale theoretical simulations in the fields of friction, adhesion and lubrication as well as in nanoscale electronics.

ACKNOWLEDGMENTS

We thank Hung-Hsiang Yang for careful reading of the manuscript. This work was supported by the Helmholtz program Science and Technology of Nanosystems (STN).

[1] C. J. Muller, J. M. van Ruitenbeek, and L. J. de Jongh, Conductance and Supercurrent Discontinuities in Atomic-Scale Metallic Constrictions of Variable Width, Phys. Rev. Lett. **69**, 140 (1992).

[2] G. Rubio, N. Agraït, and S. Vieira, Atomic-Sized Metallic Contacts: Mechanical Properties and Electronic Transport, Phys. Rev. Lett. **76**, 2302 (1996).

[3] E. Scheer, P. Joyez, M. H. Devoret, D. Esteve, and C. Urbina, What are Landauer's conduction channels in an atomic-size metallic contact? Superlattices Microstruct. **23**, 747 (1998).

[4] A. I. Yanson, G. R. Bollinger, H. E. van den Brom, N. Agraït, and J. M. van Ruitenbeek, Formation and manipulation of a metallic wire of single gold atoms, Nature (London) **395**, 783 (1998).

[5] H. E. v. d. Brom, A. I. Yanson, and J. M. v. Ruitenbeek, Characterization of individual conductance steps in metallic quantum point contacts, Phys. B **252**, 69 (1998).

[6] G. Rubio-Bollinger, S. R. Bahn, N. Agraït, K. W. Jacobsen, and S. Vieira, Mechanical Properties and Formation Mechanisms of a Wire of Single Gold Atoms, Phys. Rev. Lett. **87**, 026101 (2001).

[7] N. Agraït, C. Untiedt, G. Rubio-Bollinger, and S. Vieira, Onset of Energy Dissipation in Ballistic Atomic Wires, Phys. Rev. Lett. **88**, 216803 (2002).

[8] N. Agraït, A. L. Yeyati, and J. M. van Ruitenbeek, Quantum properties of atomic-sized conductors, Phys. Rep. **377**, 81 (2003).

[9] G. Rubio-Bollinger, P. Joyez, and N. Agraït, Metallic Adhesion in Atomic-Size Junctions, Phys. Rev. Lett. **93**, 116803 (2004).

[10] M. Dreher, F. Pauly, J. Heurich, J. C. Cuevas, E. Scheer, and P. Nielaba, Structure and conductance histogram of atomic-sized Au contacts, Phys. Rev. B **72**, 075435 (2005).

[11] J. Kröger, H. Jensen, and R. Berndt, Conductance of tip-surface and tip-atom junctions on Au(111) explored by a scanning tunnelling microscope, New J. Phys. **9**, 153 (2007).

[12] J. Kröger, N. Néel, A. Sperl, Y. F. Wang, and R. Berndt, Single-atom contacts with a scanning tunnelling microscope, New J. Phys. **11**, 125006 (2009).

[13] M. Müller, C. Salgado, N. Néel, J. J. Palacios, and J. Kröger, Plasticity of single-atom Pb junctions, Phys. Rev. B **93**, 235402 (2016).

[14] M. L. Trouwborst, E. H. Huisman, F. L. Bakker, S. J. van der Molen, and B. J. van Wees, Single Atom Adhesion in Optimized Gold Nanojunctions, Phys. Rev. Lett. **100**, 175502 (2008).

[15] C. Sabater, C. Untiedt, J. J. Palacios, and M. J. Caturla, Mechanical Annealing of Metallic Electrodes at the Atomic Scale, Phys. Rev. Lett. **108**, 205502 (2012).

[16] H. Kim and Y. Hasegawa, Site-Dependent Evolution of Electrical Conductance from Tunneling to Atomic Point Contact, Phys. Rev. Lett. **114**, 206801 (2015).

[17] Y.-h. Zhang, P. Wahl, and K. Kern, Quantum point contact microscopy, Nano Lett. **11**, 3838 (2011).

[18] L. Gerhard, T. K. Yamada, T. Balashov, A. F. Takács, R. J. H. Wesselink, M. Däne, M. Fechner, S. Ostanin, A. Ernst, I. Mertig, and W. Wulfhekel, Magnetoelectric coupling at metal surfaces, Nat. Nanotechnol. **5**, 792 (2010).

[19] J. Brand, N. Néel, and J. Kröger, Probing relaxations of atomic-scale junctions in the Pauli repulsion range, New J. Phys. **21**, 103041 (2019).

[20] J. V. Barth, H. Brune, G. Ertl, and R. J. Behm, Scanning tunneling microscopy observations on the reconstructed Au(111) surface: Atomic structure, long-range superstructure, rotational domains, and surface defects, Phys. Rev. B **42**, 9307 (1990).

[21] F. Hanke and J. Björk, Structure and local reactivity of the Au(111) surface reconstruction, Phys. Rev. B **87**, 235422 (2013).

[22] S. R. Bahn and K. W. Jacobsen, An object-oriented scripting interface to a legacy electronic structure code, Comput. Sci. Eng. **4**, 56 (2002).

[23] E. Bitzek, P. Koskinen, F. Gähler, M. Moseler, and P. Gumbsch, Structural Relaxation Made Simple, Phys. Rev. Lett. **97**, 170201 (2006).

[24] J. C. Cuevas, A. Levy Yeyati, A. Martín-Rodero, G. R. Bollinger, C. Untiedt, and N. Agraït, Evolution of Conducting Channels in Metallic Atomic Contacts Under Elastic Deformation, Phys. Rev. Lett. **81**, 2990 (1998).

[25] W. A. Hofer, A. Garcia-Lekue, and H. Brune, The role of surface elasticity in giant corrugations observed by scanning tunneling microscopes, Chem. Phys. Lett. **397**, 354 (2004).

[26] M. Wolloch, G. Feldbauer, P. Mohn, J. Redinger, and A. Vernes, *Ab initio* calculation of the real contact area on the atomic scale, Phys. Rev. B **91**, 195436 (2015).

[27] C. Untiedt, M. J. Caturla, M. R. Calvo, J. J. Palacios, R. C. Segers, and J. M. van Ruitenbeek, Formation of a Metallic Contact: Jump to Contact Revisited, Phys. Rev. Lett. **98**, 206801 (2007).

[28] W. Dednam, C. Sabater, M. A. Fernandez, C. Untiedt, J. J. Palacios, and M. J. Caturla, Modeling contact formation between atomic-sized gold tips via molecular dynamics, J. Phys.: Conf. Ser. **574**, 012045 (2015).

[29] L. Gerhard, K. Edelmann, J. Homberg, M. Valášek, S. G. Bahoosh, M. Lukas, F. Pauly, M. Mayor, and W. Wulfhekel, An electrically actuated molecular toggle switch, Nat. Commun. **8**, 14672 (2017).

[30] A. Sperl, J. Kröger, and R. Berndt, Direct observation of conductance fluctuations of a single-atom tunneling contact, Phys. Rev. B **81**, 035406 (2010).